Simulating the ECG of Ventricular Tachyarrhythmias

RH Clayton, AV Holden

University of Leeds, Leeds, United Kingdom

Abstract

The mechanisms of ventricular fibrillation (VF) remain poorly understood. The aim of this study was to use a computational model of ventricular activation coupled to a torso model to assess whether the ECG contains information about the underlying mechanism of VF. We calculated the simECG from current dipoles in the Auckland canine ventricular geometry using the boundary element approach. Mobile re-entry produced a simECG signal similar to ventricular tachycardia, whilst multiple wavelet re-entry and rapid focal activity produced simECG signals similar to VF. Frequency analysis showed a stable modal frequency for the simECG of mobile re-entry, reflecting repetitive re-entrant activity. In the other two simulations modal frequency increased during the first few seconds, reflecting a transition to more complex activity. This study suggests that the ECG may contain only limited information about VF mechanisms.

1. Introduction

Despite several decades of experimental and clinical investigation the electrical mechanisms underlying ventricular fibrillation (VF) remain poorly understood and sudden cardiac death remains an important health problem in the developed world. The characteristic ECG signal recorded during VF suggests rapid, self-sustaining activation, and this has been confirmed by experimental studies [1]. Several mechanisms are consistent with these features including a drifting re-entrant wave [2], a pinned re-entrant wave with fibrillatory conduction [3], multiple re-entrant waves [4], and rapid focal activity in different parts of the ventricle [5].

In this study we coupled a computational model of electrical activation during VF to a torso model, and simulated the ECG signals produced by (i) a single drifting re-entrant wave, (ii) multiple wavelet re-entry, and (iii) rapid focal activation. The aim of the study was to investigate whether the surface ECG contains information about the underlying mechanism of VF.

2. Methods

Our computational model of VF described action potential propagation in an anisotropic monodomain with the non-linear diffusion equation:

$$C_m \frac{\partial V_m}{\partial t} = \nabla \cdot \mathbf{D} \nabla V_m - I_{ion} \quad (1)$$

where V_m is voltage across the cell membrane, C_m specific membrane capacitance, $\boldsymbol{D}$ a diffusion tensor and I_{ion} current flow though the cell membrane per unit area.

2.1. Computational model of VF

We used the Fenton-Karma (FK) equations to generate the membrane patch current I_{ion} [6]. We set the model parameters to the values given in Table 1 of [6] to give the action potential duration (APD) and conduction velocity (CV) restitution of either the modified Beeler-Reuter (mBR) model (with k set to 1.0) or the Beeler-Reuter (BR) model.

We set C_m to 1 $\mu F\ cm^{-2}$ and integrated equation (1) using a simple explicit Euler scheme with a time step (Δt) of 0.1 ms, a space step (Δ) of 0.33 mm and no flux boundary conditions at each surface. We set the diffusion coefficients parallel to and perpendicular to the fibre direction to be $D_{\parallel} = 0.2\ mm^2 ms^{-1}$ and $D_{\perp} = 0.05\ mm^2 ms^{-1}$ respectively, and these values gave a plane wave speed of $0.64\ ms^{-1}$ along fibres and $0.28\ ms^{-1}$ across fibres.

We used the detailed canine ventricular anatomy and fibre orientation from the University of Auckland (http://www.cmiss.org). The finite element description of both shape and fibre orientation were sampled on a regular Cartesian grid with a spacing of 0.33 mm to give a ventricular geometry with 5 567 778 grid points.

We initiated re-entry with a single transmural filament by activating part of the basal left ventricular (LV) free wall while maintaining a line of block running from base to apex for 120 ms. With mBR restitution we obtained a stable, drifting re-entrant wave, and with BR restitution we obtained an unstable re-entrant wave that broke down to multiple wavelet re-entry. For rapid focal activation we applied a stimulus to randomly chosen locations in the ventricles every 5 ms.

0276–6547/02 $17.00 © 2002 IEEE

Computers in Cardiology 2002;29:321–324.

2.2. Torso model

A full description of our approach to simulating the surface ECG is given elsewhere [7]. Briefly, we used the boundary element method (BEM) to estimate the body surface potential Φ as a function of position $\mathbf{r}$, assuming the torso can be approximated as a homogeneous and isotropic volume conductor. Using Green's theorem, the potential resulting from an impressed current density $\mathbf{J}^i$ can be given by [8]

$$\Phi(\mathbf{x}) = \frac{1}{4\pi\sigma}\int_V \frac{1}{r}\nabla\cdot\mathbf{J}^i \, dV + \frac{1}{4\pi}\int_S \Phi\frac{\mathbf{r}}{r^3}\cdot\mathbf{ds} \,, \qquad (2)$$

where $\mathbf{x}$ is the position vector of the observation point, in the first term r is the distance from each volume element dV to the observation point $\mathbf{x}$, and in the second term $\mathbf{r}$ is the vector from $\mathbf{x}$ to the surface element $\mathbf{ds}$.

Figure 1. Triangulated torso geometry, location of canine ventricles, and location of 12 lead ECG electrodes.

We approximated the impressed current density $\mathbf{J}^i$ by

$$\mathbf{J}^i = \sigma_k \nabla V_m \quad , \qquad (3)$$

where V_m was obtained from the action potential propagation model at 1 ms intervals. For the computation we rewrote equation 2 in discrete form [8]

$$\frac{\Phi_i}{2} - \sum_{j=1, j\neq i}^{N} \frac{\Delta\Omega_j}{4\pi}\Phi_j = \frac{1}{4\pi\sigma}\sum_{k=1}^{M}\frac{\nabla\cdot\mathbf{J}_k^i}{r}\delta V \,, \qquad (4)$$

where $\mathbf{J}^i$ was made up of M discrete dipoles each occupying a volume δV, and the torso surface of N discrete triangles. Φ_i was the potential in the centre of triangle i, $\Delta\Omega_j$ the solid angle of the j^{th} triangle as seen from i [9], and r the distance from each dipole to triangle i. For $i=j$, $\Delta\Omega = 2\pi$, so we could rewrite equation 4 in matrix form, and solve it using back substitution and LU decomposition [7, 10].

We used a finite element male torso geometry [11] that was kindly provided by the University of Auckland (http://www.cmiss.org) and is segmented into heart, lungs, muscle layer and subcutaneous fat. We divided the surface of the torso region into 2016 triangles, and selected 10 triangles as the sites of ECG electrodes for calculating a 12 lead simECG. The ventricular geometry was inserted into the torso and oriented so that the long axis (base to apex) made an angle of 35° with the transverse plane and 30° with the sagittal plane. Using this orientation the canine ventricular geometry was both aligned with and fitted inside the human ventricles that are part of the torso dataset. Figure 1 shows the triangulated surface geometry, with the location of the ventricles and simECG electrodes also indicated.

3. Results

Snapshots from simulated drifting re-entry are shown in Figure 2, and the simulated ECG signals from this simulation are shown in Figure 3.

Figure 2. Isosurfaces showing active tissue 100 ms (left), 1000 ms (middle) and 2000 ms (right) after initiation of drifting re-entry in the LV free wall.

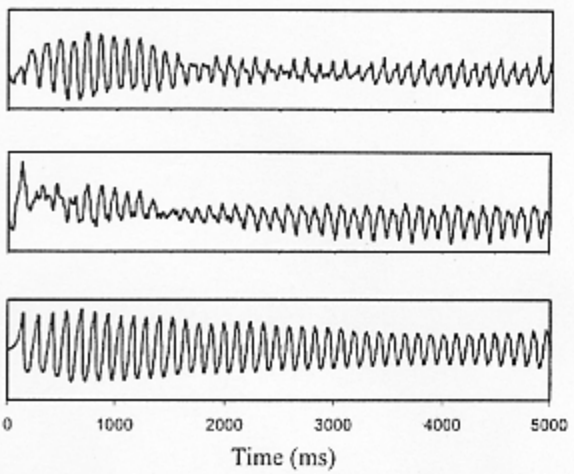

Figure 3. Simulated ECG produced by drifting re-entrant wave showing Leads I (top) aVF (middle) and V1 (bottom).

During the first two seconds of activity the re-entrant wave drifted towards the posterior LV free wall, and this drift produced pronounced amplitude changes in simECG leads I and VF, with only small changes in V1. The intervals between simECG peaks were consistently about 140 ms, and corresponded exactly with the period of re-entry.

Figures 4 and 5 show isosurfaces and simECG signals for the multiple wavelet simulation. The initial re-entrant wave in the LV free wall broke down after about four rotations (about 500 ms) and some evidence of this transition to more complex activation can be seen as a change in amplitude and interval between complexes in the simECG signals.

Figure 4. Isosurfaces showing active tissue 100 ms (left), 1000 ms (middle) and 2000 ms (right) after initiation of multiple wavelet re-entry in the LV free wall.

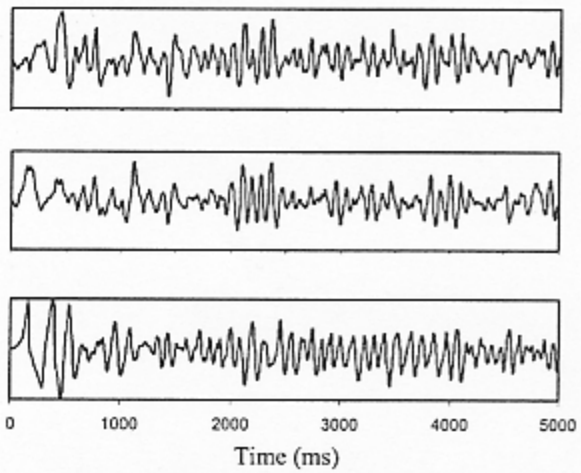

Figure 5. Simulated ECG produced by multiple wavelets showing Leads 1 (top) aVF (middle) and V1 (bottom).

Figures 6 and 7 show isosurfaces and simECG signals for the simulation with rapid focal activity. These signals also show a transition from slower to faster activity.

Frequency analysis of each 1 s epoch showed differences between the simECG of drifting re-entry and the simECG of both multiple wavelet re-entry and rapid focal activity. The modal frequencies of spectra in each simulation are shown in Figure 8. The repetitive activity resulting from the drifting re-entrant wave results in an almost constant modal frequency, whereas the increasingly complex activity in the other two simulations results in an increasing modal frequency that is similar to findings from frequency analysis of clinical VF episodes [12].

Figure 6. Isosurfaces showing active tissue 100 ms (left), 1000 ms (middle) and 2000 ms (right) after initiation of rapid focal activity.

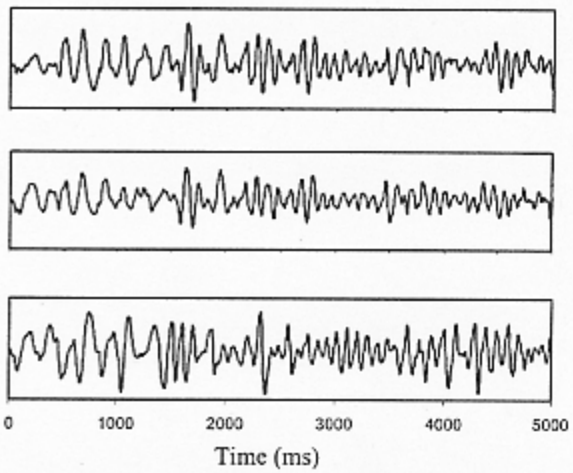

Figure 7. Simulated ECG produced by rapid focal activity showing Leads 1 (top) aVF (middle) and V1 (bottom).

4. Discussion

This preliminary study has shown that it is possible to couple computational models of ventricular electrical activation to a torso model, and hence to obtain simulated ECG signals produced by specific mechanisms of arrhythmia.

We have shown that a drifting but stable re-entrant wave produced simECG signal that was similar to polymorphic ventricular tachycardia. More complex activation patterns sustained by multiple wavelet re-entry and rapid focal activity produced simECG signals that resembled VF.

Using a simple frequency analysis technique, the simECGs produced by multiple wavelet re-entry and rapid focal activity could not be easily distinguished. More sophisticated signal processing techniques that quantify the phase relationship between the individual leads may be able to distinguish between these

mechanisms. However this study does suggest that it may be difficult to distinguish between different mechanisms using the body surface ECG alone.

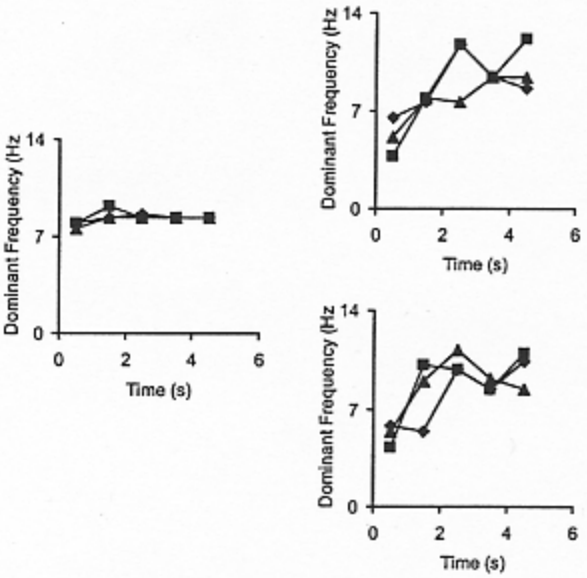

Figure 8. Modal frequencies of simECG leads I (diamonds) aVF (squares), and V1 (triangles) for drifting re-entry (left), multiple wavelets (top right) and rapid focal activity (bottom right).

Acknowledgements

This work has been supported by the British Heart Foundation through the award of Basic Science Lectureship BS98001 to RHC. We are also grateful to the UK EPSRC and MRC for additional funding.

References

[1] Winfree AT, (Ed). Focus issue: Fibrillation in normal ventricular myocardium. Chaos 1998;8:1-241.

[2] Gray RA, Jalife J, Panfilov A, Baxter WT, Cabo C, Davidenko JM, Pertsov AM. Nonstationary vortexlike reentrant activity as a mechanism of polymorphic ventricular tachycardia in the isolated rabbit heart. Circulation 1995;91:2454-2469.

[3] Zaitsev AV, Berenfeld O, Mironov SF, Jalife J, Pertsov AM. Distribution of excitation frequencies on the epicardial and endocardial surfaces of fibrillating ventricular wall of the sheep heart. Circulation Research 2000;86:408-417.

[4] Valderrabano M, Lee MH, Ohara T, Lai AC, Fishbein MC, Lin SF, Karagueuzian HS, Chen PS. Dynamics of intramural and transmural reentry during ventricular fibrillation in isolated swine ventricles. Circulation Research 2001;88:839-848.

[5] Pogwizd SM, Corr PB. The contribution of nonreentrant mechanisms to malignant ventricular arrhythmias. Basic Research in Cardiology 1992;87:115-129.

[6] Fenton F, Karma A. Vortex dynamics in three-dimensional continuous myocardium with fibre rotation: Filament instability and fibrillation. Chaos 1998;8:20-47.

[7] Clayton RH, Holden AV. Computational framework for simulating the mechanisms and ECG of re-entrant ventricular fibrillation. Physiological Measurement 2002;(In press).

[8] Barr RC, Pilkington TC, Boineau JP, Spach MS. Determining surface potentials from current dipoles, with application to electrocardiography. IEEE Transactions on Biomedical Engineering 1966;13:88-92.

[9] van Oosterom A, Strackee J. The solid angle of a plane triangle. IEEE Transactions on Biomedical Engineering 1983;30:125-126.

[10] Salu Y. Implementing a consistency criterion in numerical solution of the bioelectric forward problem. IEEE Transactions on Biomedical Engineering 1980;27:338-341.

[11] Bradley CP, Pullan A, Hunter PJ. Geometric modelling of the human torso using cubic hermite elements. Annals of Biomedical Engineering 1997;25:96-111.

[12] Clayton RH, Murray A, Campbell RWF. Changes in the surface electrocardiogram during the onset of spontaneous ventricular fibrillation in man. European Heart Journal 1994;15:184-188.

Address for correspondence:

Dr Richard H Clayton,
School of Biomedical Sciences,
Worsley Building, University of Leeds,
Leeds LS2 9JT
United Kingdom

Email:
richard@cbiol.leeds.ac.uk